

Electric field effect of GaAs monolayer from first principles

Jiongyao Wu, Yali Yang, Heng Gao, Yuting Qi, Jiaqi Zhang, Zhenhua Qiao, and Wei Ren

Citation: *AIP Advances* **7**, 035218 (2017);

View online: <https://doi.org/10.1063/1.4979507>

View Table of Contents: <http://aip.scitation.org/toc/adv/7/3>

Published by the [American Institute of Physics](#)

Articles you may be interested in

[Spin magnetic susceptibility of ferromagnetic silicene in the presence of Rashba spin-orbit coupling](#)

AIP Advances **7**, 035211 (2017); 10.1063/1.4978052

[Understanding the microwave annealing of silicon](#)

AIP Advances **7**, 035214 (2017); 10.1063/1.4978912

[Ab initio molecular dynamics study of temperature and pressure-dependent infrared dielectric functions of liquid methanol](#)

AIP Advances **7**, 035115 (2017); 10.1063/1.4978899

[Effects of surface roughness on scratch resistance and stress-strain fields during scratch tests](#)

AIP Advances **7**, 035217 (2017); 10.1063/1.4979332

[Study of ultraviolet-visible light absorbance of exfoliated graphite forms](#)

AIP Advances **7**, 035323 (2017); 10.1063/1.4979607

[Negative thermal expansion properties in tetragonal NbPO₅ from the first principles studies](#)

AIP Advances **7**, 035202 (2017); 10.1063/1.4977874

HAVE YOU HEARD?

Employers hiring scientists and
engineers trust

PHYSICS TODAY | JOBS

www.physicstoday.org/jobs



Electric field effect of GaAs monolayer from first principles

Jiongyao Wu,¹ Yali Yang,¹ Heng Gao,¹ Yuting Qi,¹ Jiaqi Zhang,¹
Zhenhua Qiao,² and Wei Ren^{1,a}

¹*Department of Physics, International Center for Quantum and Molecular Structures, and Materials Genome Institute, Shanghai University, Shanghai 200444, China*

²*ICQD, Hefei National Laboratory for Physical Sciences at Microscale, Synergetic Innovation Centre of Quantum Information and Quantum Physics, CAS Key Laboratory of Strongly-Coupled Quantum Matter Physics and Department of Physics, University of Science and Technology of China, Hefei, Anhui 230026, China*

(Received 25 January 2017; accepted 19 March 2017; published online 27 March 2017)

Using first-principle calculations, we investigate two-dimensional (2D) honeycomb monolayer structures composed of group III-V binary elements. It is found that such compound like GaAs should have a buckled structure which is more stable than graphene-like flat structure. This results a polar system with out-of-plane dipoles arising from the non-planar structure. Here, we optimized GaAs monolayer structure, then calculated the electronic band structure and the change of buckling height under external electric field within density functional theory using generalized gradient approximation method. We found that the band gap would change proportionally with the electric field magnitude. When the spin-orbit coupling (SOC) is considered, we revealed fine spin-splitting at different points in the reciprocal space. Furthermore, the valence and conduction bands spin-splitting energies due to SOC at the K point of buckled GaAs monolayers are found to be weakly dependent on the electric field strength. Finally electric field effects on the spin texture and second harmonic generation are discussed. The present work sheds light on the control of physical properties of GaAs monolayer by the applied electric field. © 2017 Author(s). All article content, except where otherwise noted, is licensed under a Creative Commons Attribution (CC BY) license (<http://creativecommons.org/licenses/by/4.0/>). [<http://dx.doi.org/10.1063/1.4979507>]

INTRODUCTION

Since the discovery of graphene as a freestanding monoatomic layer,¹ more and more layered two-dimensional (2D) materials have been studied, such as monolayers of molybdenum disulfide (MoS₂),^{2,3} black phosphorus⁴ and functionalized graphene.^{5–10} In particular, graphene is a 2D honeycomb structure of carbon with unique symmetry, which gives rise to the energy band structure of the Dirac points at the Fermi level.^{1,11,12} The discovery of graphene also allowed us to observe the quantum Hall effect using the graphene layered devices.^{13,14} Silicene is predicted to be a stable 2D allotrope of silicon with a buckled hexagonal structure closely related to the structure of graphene.¹⁵ The properties of silicene have been studied intensively very recently, whose hexagonal honeycomb structure also gives rise to the linear dispersion relation in band structure. On the other hand, silicene may be implemented with the silicon technology and the buckled geometry may offer some excellent properties beyond the graphene. For instance, an external electric field opens band gap in silicene but not in graphene.¹⁶ The monolayer geometry of group III-V binary compounds¹⁷ are structurally similar to the group IV silicene. The buckled monolayer structure with trigonal symmetry is more stable with respect to the planar geometry. This is due to the destabilization of the π bonds in the sp^2 hybridization because of the different chemistry between two neighboring atoms. When spin-orbit

^aEmail: renwei@shu.edu.cn



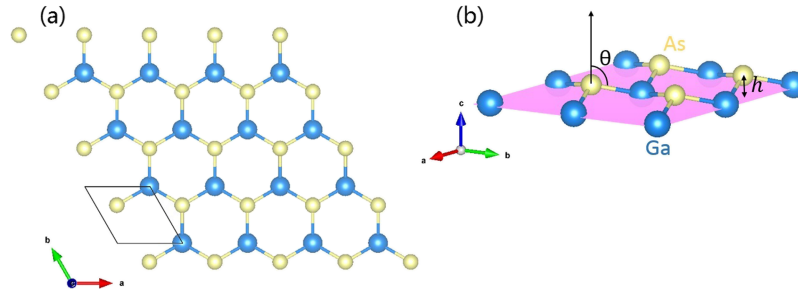


FIG. 1. Monolayer structure composed of binary elements GaAs. (a) Top view of a buckled GaAs monolayer along the c -axis. (b) Side view of a buckled GaAs monolayer, where the cations Ga (blue) plane is separated by a distance h from anion As (yellow) plane. The buckling angle θ is defined as the angle between the Ga-As bond and the c -axis direction.

coupling is considered, both graphene and silicene can have finite band gaps as Kane-Mele 2D topological insulator.¹⁸ For buckled germanium monolayer, spin-orbit coupling may even open a much larger band gap.¹⁹

Using first-principles calculations, Şahin *et al.* investigated 2D honeycomb structures of group-IV elements and of group III-V elements.²⁰ Recently, there have been a lot of reports on group III-V compounds,²¹ for instance, 2D hexagonal boron-nitride (h-BN) honeycomb structure^{22,23} is an insulating isomorph of graphene with a large band gap of about 6 eV, as an ideal candidate for dielectric substrates and tunnel barriers.^{24–27} Other than that, it was found that many other 2D III-V compounds were buckled honeycomb, and such AB monolayers have trigonal symmetry (e.g., group IV binary monolayers SiGe, SiSn, GeSn and group III-V binary monolayers AlSb, GaP, GaAs, InP, InAs, InSb), see the Fig. 1. These group III-V binary AB monolayers are polar semiconductors with the presence of the electronegativity difference and dipole moment at each A-B bond. All the structures have the spin-orbit coupling (SOC) induced spin-splitting in valence and conduction bands at the high-symmetry K point. Although the systems are nonmagnetic, electrons around K valley experience strong Zeeman-like magnetic field. The spin polarization may be switched by changing the spatial buckling orientation, or by changing the time-reversed K and $-K$ points. The spin-valley coupled physics properties in two-dimensional honeycomb binary compounds provide us possibility for exploring new quantum materials. In this work, we investigate the electric field effects on the electronic properties of buckled 2D GaAs monolayer.

METHODS

We have performed first-principle calculations for structure relaxation, total energy and electronic structures. All calculations were done by using density functional theory (DFT) at the PBE level²⁸ unless otherwise stated, in which the exchange-correlation potential is approximated by generalized gradient approximation (GGA). A set of $(7 \times 7 \times 1)$ k -point sampling is used for Brillouin zone in the reciprocal space, and the k -point mesh is generated by Monkhorst-Pack scheme.²⁹ The energy cutoff is 500 eV, and the convergence criterion of self-consistent calculations is 10^{-8} eV for total-energy values. Fermi level smearing is taken as 0.05 eV for geometry optimization and the same value for energy band calculations. All atomic positions and unit cell were optimized until the atomic forces were less than 0.005 eV/Å. The supercell contains a minimal vacuum spacing of 20 Å to prevent interactions between the adjacent periodic layers. To consider the buckling height and band gap values obtained by PBE, we also carried out calculations based on LDA³⁰ and PBEsol³¹ exchange correlation potential. Moreover, we study the important SOC effect by considering the relativistic correction in the pseudopotential DFT calculations, as implemented in the Vienna Ab Initio Simulation Package (VASP).

We calculate the second harmonic generation (SHG) to study its dependence on the buckling structure change. The SHG spectra of the second order susceptibility tensor are obtained by using the “exciting” software,³² which is a full-potential all-electron DFT package to calculate the many physical properties of condensed matters.

RESULTS AND DISCUSSION

We begin our analysis by confirming the 2D buckled monolayer structures of trigonal symmetry, namely group IV binary monolayers SiGe, SiSn, GeSn and group III-V binary monolayers AlSb, GaP, GaAs, InP, InAs, InSb. The calculated buckling angle θ (deg), height h (Å), band gaps (eV) and spin-splitting energies of valence band (conduction band) ΔE_{VB} (ΔE_{CB}) (meV) at the K point are in good agreement with Ref. 17, 20. We note that group-IV AB compounds generally have band gaps smaller than those of III-V groups. Group III-V compound semiconductors are important for making the light emitting diode, and for the solar cell materials. Among them the GaAs is the representative, thus in the following we focus our attention on the physical properties of GaAs and the electric field effects. In Fig. 2, we illustrate the electronic band structures of GaAs monolayer with and without taking SOC³³ into account. The first Brillouin zone of the hexagonal primitive cell is used in our electronic structure calculation. From both results with and without SOC, we obtain a semiconductor with a band gap of 1.09 eV. The valence band maximum (VBM) is located at the high-symmetry K point of the Brillouin zone, whereas the conduction band minimum (CBM) is located at the high-symmetry Γ point. The VBM at K point is slightly higher than Γ point by 0.01 eV, and our PBEsol functional results show both VBM and CBM are located at Γ point. In addition, we find that both the valence and conduction bands are splitted by SOC at K point, but the states are degenerate at the high-symmetry M point. The spin splitting at M point is so-called Rashba-like³⁴ along horizontal axis direction, and at K point it is Zeeman-like along the vertical energy scale. Furthermore, as shown in the insets of Fig. 2, the spin splitting value ΔE_{VB} at the K point in GaAs is found to be 13.6 meV, and the spin splitting value ΔE_{CB} at the K point is 34.2 meV.

The electric field tunes the carrier concentration in a semiconductor device, so that electron transport through it can be controlled. Now we discuss the change of physical properties by external electric field effect³⁵ on our 2D system. The buckling height can be modified by the external electric field along c axis, as shown in the Fig. 3. Although we get different values of buckling from the GGA, LDA and PBEsol calculations, the electric field induced buckling variations have the same trend in all cases. When the monolayer structure is under positive electric field, the heights increase linearly by about 0.02 Å when the field strength is 0.6 eV/Å. On the other hand, when we switch the electric field along the opposite c axis, the buckling height decreases linearly, with the same range of change about 0.02 Å. In the monolayer structure of GaAs, there is an internal equivalent field E_{int} which is along the c axis direction. The positive external electric field assists to increase the E_{int} within the structure, so the height of GaAs monolayer could be increased. When the reversed external electric field is applied, it effectively decreases the E_{int} within the GaAs structure, so the height would be decreased. This field-induced structural change has impact on the Ga-As bond length

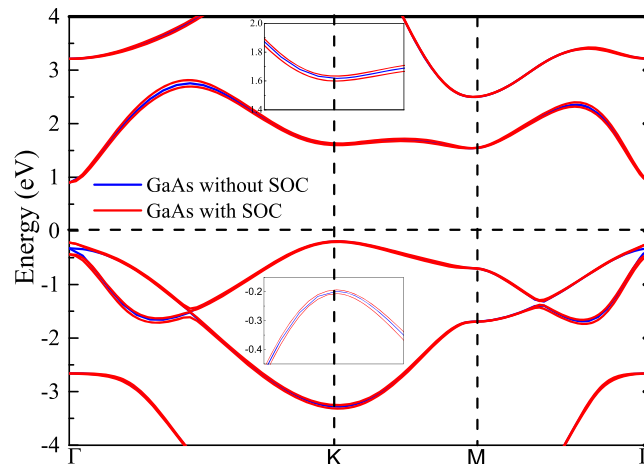


FIG. 2. Band structures of GaAs monolayer without (blue) and with (red) spin-orbit coupling (SOC). The calculated band gap is 1.09 eV, from the valence band maximum (VBM) at K point to the conduction band minimum (CBM) at Γ point. The insets show the valence and conduction bands splitting zoom-in at K points.

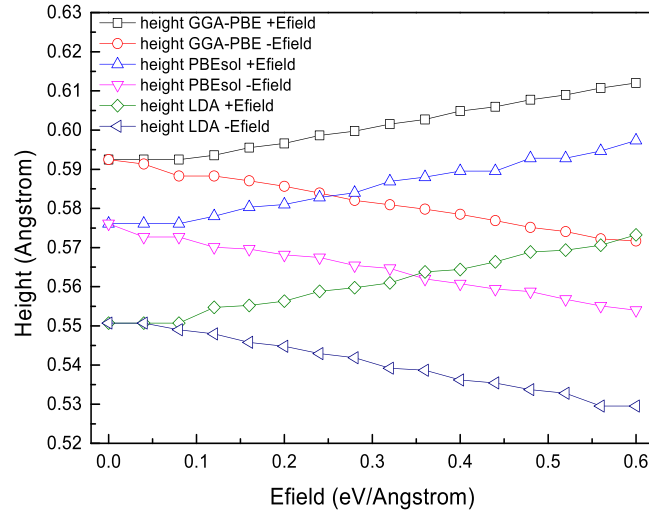


FIG. 3. The buckling height values changed by the electric field with direction parallel and antiparallel to the c axis without SOC. Inclusion of SOC gives same structural change results.

and angle change, and consequently we expect the band gap should also have a response to the electric field.

The lattice parameter $a=b=4.0557\text{\AA}$ under zero electric field, and the positive electric field of 0.56 eV/\AA may change the lattice parameter to $a=b=4.0536\text{ \AA}$; whereas lattice parameters ($a=b$) are increased from 4.0557 \AA to 4.0609 \AA , under the negative electric field of 0.52 eV/\AA . This can be understood that the change by the positive and negative external electric field is effectively applying a stress along ab plane, such that the bond with a mixed covalent bond to ionic character shows a reverse piezoelectric-like phenomenon in GaAs monolayer.

In Fig. 4, we present the electric field induced change of band gap,³⁶ with and without SOC. When SOC is not considered, the band gap amplitudes are increased proportionally to the field strength, with the direction of electric field along the positive c axis. Similar to the height variation trend, the band gap is linearly enhanced by 0.03 eV when the field strength is 0.6 eV/\AA . For the electric field of opposite direction, the band gap values are suppressed by about 0.06 eV under electric field of -0.6 eV/\AA . Therefore the buckling height value is correlated with the band gaps under the externally applied electric field. Such field effect is dramatically affected by the SOC inclusion in the calculation. Fig. 4 show that the positive external electric field very slightly increases the band gap, and then decreases the band gap. Meanwhile we have found that the indirect band gap between K and Γ points can be changed to a direct band gap at Γ point. On the other hand, the negative external electric field decreases band gap with SOC more dramatically, and further negative electric field is found to close the band gap. This effect is confirmed by using different functionals, which give us a critical electric field for gap closing at about 0.5 eV/\AA . In the inset of Fig. 4 we present two band structures to show how the conduction bands are splitted and shifted down below the Fermi level near Γ point.

We calculate the change of bands spin-splitting due to SOC, now in the presence of external electric field. For that, the spin-splitting energy values ΔE_{VB} (meV) and ΔE_{CB} (meV) of valence band and conduction band at the K point are shown in Fig. 5. Under the positive external electric field of 0.5 eV/\AA , we can see that the ΔE_{VB} increases from 13.6 meV to 14.0 meV ; for the negative field of 0.5 eV/\AA , the ΔE_{VB} decreases from 13.6 meV to 13.1 meV . Similar behaviors are found for the conduction band spin-splitting (ΔE_{CB}) at K point. The positive/negative electric field increases/decreases ΔE_{VB} from 34.2 meV to $34.4/33.8\text{ meV}$.

The external electric field might not be able to switch the displaced positions of Ga and As atoms in the buckled GaAs monolayer, if the energy barrier is too large for ferroelectric-type structural inversion. Nonetheless we have made another monolayer configuration of opposite polarization by manual operation. The height of this equally stable degenerate structure is also equal to that in Fig. 1, but now the Ga atomic layer is above As layer with a same height of 0.6 \AA . Then we calculated

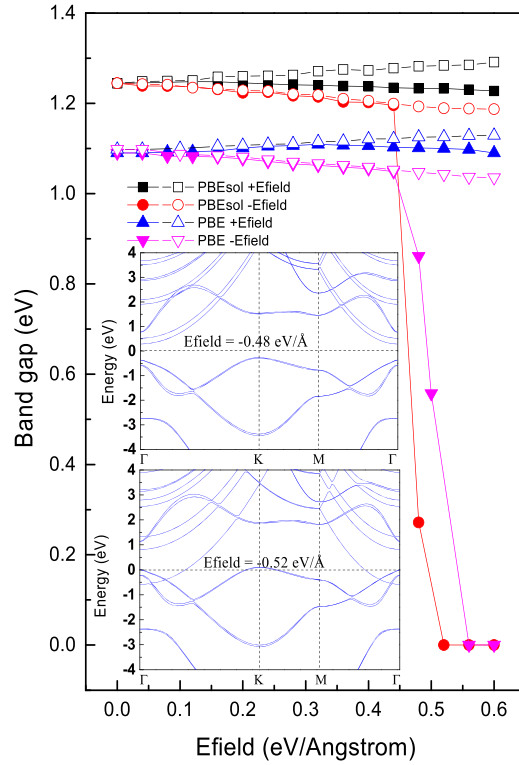


FIG. 4. The band gap change by the positive and negative external electric fields along the c axis direction. The band structures with SOC show gap closing effect at a critical field strength of about 0.5 eV/\AA . Solid symbols are for calculations with SOC, unfilled symbols are for calculations without SOC.

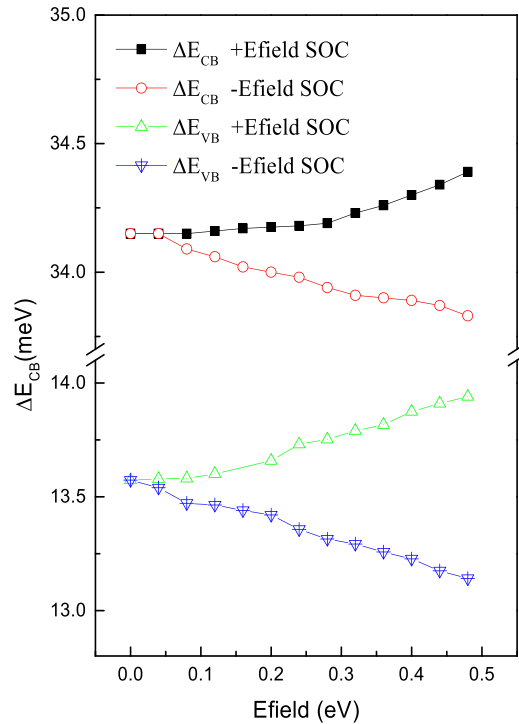


FIG. 5. The change of valence (conduction) band spin-splitting energies ΔE_{VB} (ΔE_{CB}) with SOC by positive and negative electric field.

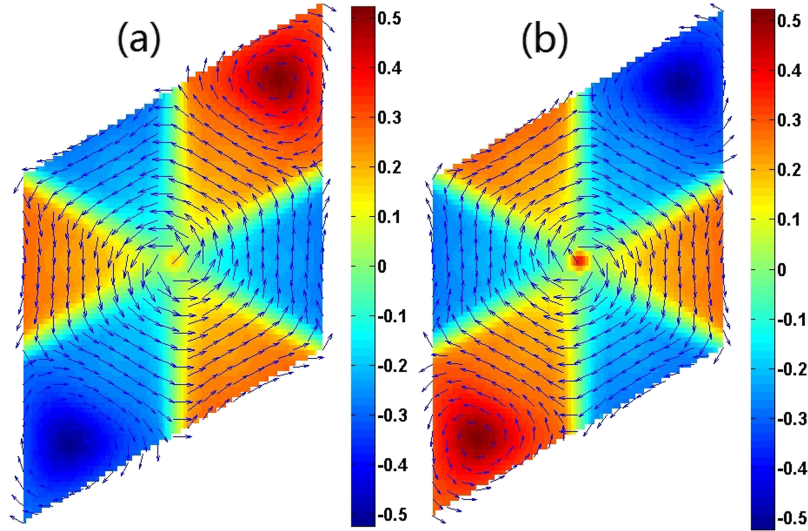


FIG. 6. (a) The spin textures of the GaAs structure in Fig. 1 (As above Ga) and (b) the inverted GaAs structure (Ga above As) for states of VBs (0.18eV below the Fermi level) for the whole Brillouin zone.

spin textures of the two structures VBs (0.18eV below the Fermi level) spin-splitting in the Brillouin zone. Fig. 6(a) is the spin-texture of the initial structure in Fig. 1 without external electric field, where the directions of VBs spins are rotating anticlockwise in the reciprocal space. Fig. 6(b) is the spin-texture of the inverted structure again without external electric field, now the direction of VBs spins form a clockwise vortex in the k-space. Besides this chirality inversion, we can see that the z-components of spins are also completely switched by the change of structure polarity. The breaking of inversion symmetry in our bipartite monolayer thus provides us great opportunity to study the emerging spin-valley-sublattice coupling dependent physics.

Finally we calculate the second harmonic generation spectra of GaAs two-dimensional structures with different buckling strength, as shown in Fig. 7. For the flat monolayer $h=0\text{\AA}$, the calculated second-order nonlinear susceptibility is equal to 0 nm/V because of the symmetry of this structure. The effective bulk-like second-order susceptibility of the GaAs monolayers, can be defined as $d_{eff} = \chi^{(2)}/2T$, where T is the thickness of a GaAs monolayer. When we use DFT to calculate the SHG spectra, the input parameters are carefully checked including the lattice constant, coordinate of each atom, K-mesh and so on. In this paper we calculate the SHG spectra of GaAs monolayer of different heights (0, 0.12, 0.24, 0.36, 0.48 and 0.6 \AA). For that, we take the initial GaAs structure in Fig. 1 to find the best K-mesh for all calculations. From a tradeoff between the computational expense and precision, we select the $32 \times 32 \times 1$ K-mesh for the following calculations. The calculated second-order

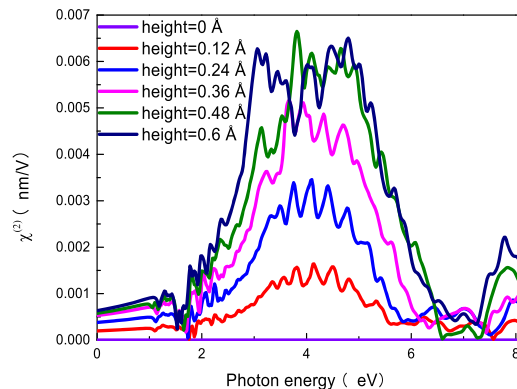


FIG. 7. The SHG spectra of GaAs two-dimensional structures with different buckling heights. The values of buckling height are 0, 0.12, 0.24, 0.36, 0.48 and 0.6 \AA .

nonlinear optical susceptibility $\chi^{(2)}$ values are generally increased by the buckling height after the symmetry is broken. In particular, the low energy excitations are significantly enhanced with the prominent peaks appearing near the visible light region. The predicted SHG spectra of monolayers with different thickness can be employed to probe the relationship between buckling structural change and optical properties of the 2D materials in general.

CONCLUSION

In summary, we investigate the physical properties of buckled GaAs monolayers, taking into account the roles of spin-orbit coupling and external electric field. Even the external electric field might not be able to induce polar structural inversion, it can modify delicately the buckling amplitude and electronic structure. When SOC is absent, the buckling height and band gap would linearly increase or decrease by positive or negative external electric field. When we consider the SOC-induced band spin-splitting, the band gap and band splitting values have different dependence on the external electric field. Furthermore, we have also present the interesting spin texture and second harmonic generation spectra from the first principles, and predict some electric field effect to be investigated in future experiments.

ACKNOWLEDGMENTS

This work was supported by the National Key Basic Research Program of China (2015CB921600), the National Natural Science Foundation of China (11274222, 51672171), the Eastern Scholar Program from the Shanghai Municipal Education Commission. Special Program for Applied Research on Super Computation of the NSFC-Guangdong Joint Fund (the second phase) is also acknowledged.

- ¹ K. S. Novoselov *et al.*, “Two-dimensional gas of massless Dirac fermions in graphene,” *Nature* **438**, 197–200 (2005).
- ² H. Zeng, J. Dai, W. Yao, D. Xiao, and X. Cui, “Valley polarization in MoS₂ monolayers by optical pumping,” *Nat Nanotechnol* **7**, 490–493 (2012).
- ³ H. Qiu *et al.*, “Hopping transport through defect-induced localized states in molybdenum disulphide,” *Nat Commun* **4**, 2642 (2013).
- ⁴ X. Chen *et al.*, “Probing the electronic states and impurity effects in black phosphorus vertical heterostructures,” *2D Materials* **3**, 015012 (2016).
- ⁵ X. Zheng *et al.*, “Fluorinated graphene in interface engineering of Ge-based nanoelectronics,” *Advanced Functional Materials* **25**, 1805–1813 (2015).
- ⁶ Y. Yang, W. Ren, and L. Bellaiche, “Properties of hydrofluorinated carbon- and boron nitride-based nanofilms: A first-principles study,” *Physical Review B* **89** (2014).
- ⁷ W.-M. Huang, J.-M. Tang, and H.-H. Lin, “Power-law singularity in the local density of states due to the point defect in graphene,” *Physical Review B* **80** (2009).
- ⁸ C. Park *et al.*, “Electronic properties of bilayer graphene strongly coupled to interlayer stacking and an external electric field,” *Phys Rev Lett* **115**, 015502 (2015).
- ⁹ E. Pop, V. Varshney, and A. K. Roy, “Thermal properties of graphene: Fundamentals and applications,” *MRS Bulletin* **37**, 1273–1281 (2012).
- ¹⁰ A. Rycerz, J. Tworzydło, and C. W. J. Beenakker, “Valley filter and valley valve in graphene,” *Nat Phys* **3**, 172–175 (2007).
- ¹¹ G. Giovannetti, P. A. Khomyakov, G. Brocks, P. J. Kelly, and J. van den Brink, “Substrate-induced band gap in graphene on hexagonal boron nitride: *Ab initio* density functional calculations,” *Physical Review B* **76** (2007).
- ¹² W. Ren, T. H. Cho, T. C. Leung, and C. T. Chan, “Gated armchair nanotube and metallic field effect,” *Applied Physics Letters* **93**, 142102 (2008).
- ¹³ Y. Zhang, Y. W. Tan, H. L. Stormer, and P. Kim, “Experimental observation of the quantum Hall effect and Berry’s phase in graphene,” *Nature* **438**, 201–204 (2005).
- ¹⁴ K. S. Novoselov *et al.*, “Room-temperature quantum Hall effect in graphene,” *Science* **315**, 1379 (2007).
- ¹⁵ L. C. Lew Yan Voon, J. Zhu, and U. Schwingenschlögl, “Silicene: Recent theoretical advances,” *Applied Physics Reviews* **3**, 040802 (2016).
- ¹⁶ N. D. Drummond, V. Zolyomi, and V. I. Fal’ko, “Electrically tunable band gap in silicene,” *Physical Review B* **85** (2012).
- ¹⁷ D. Di Sante, A. Stroppa, P. Barone, M.-H. Whangbo, and S. Picozzi, “Emergence of ferroelectricity and spin-valley properties in two-dimensional honeycomb binary compounds,” *Physical Review B* **91** (2015).
- ¹⁸ C. C. Liu, W. Feng, and Y. Yao, “Quantum spin Hall effect in silicene and two-dimensional germanium,” *Phys Rev Lett* **107**, 076802 (2011).
- ¹⁹ C.-C. Liu, H. Jiang, and Y. Yao, “Low-energy effective Hamiltonian involving spin-orbit coupling in silicene and two-dimensional germanium and tin,” *Physical Review B* **84** (2011).

- ²⁰ H. Şahin *et al.*, “Monolayer honeycomb structures of group-IV elements and III-V binary compounds: First-principles calculations,” *Physical Review B* **80** (2009).
- ²¹ T. F. Kuech, “III-V compound semiconductors: Growth and structures,” *Progress in Crystal Growth and Characterization of Materials* **62**, 352–370 (2016).
- ²² S. Azevedo, J. R. Kaschny, C. M. de Castilho, and B. Mota Fde, “A theoretical investigation of defects in a boron nitride monolayer,” *Nanotechnology* **18**, 495707 (2007).
- ²³ A. Dankert, M. Venkata Kamalakar, A. Wajid, R. S. Patel, and S. P. Dash, “Tunnel magnetoresistance with atomically thin two-dimensional hexagonal boron nitride barriers,” *Nano Research* **8**, 1357–1364 (2014).
- ²⁴ P. J. Zomer, S. P. Dash, N. Tombros, and B. J. van Wees, “Transfer technique for high mobility graphene devices on commercially available hexagonal boron nitride,” *Applied Physics Letters* **99**, 232104 (2011).
- ²⁵ C. R. Dean *et al.*, “Boron nitride substrates for high-quality graphene electronics,” *Nat Nanotechnol* **5**, 722–726 (2010).
- ²⁶ G.-H. Lee *et al.*, “Electron tunneling through atomically flat and ultrathin hexagonal boron nitride,” *Applied Physics Letters* **99**, 243114 (2011).
- ²⁷ L. Britnell *et al.*, “Electron tunneling through ultrathin boron nitride crystalline barriers,” *Nano Lett* **12**, 1707–1710 (2012).
- ²⁸ B. Hammer, L. B. Hansen, and J. K. Nørskov, “Improved adsorption energetics within density-functional theory using revised Perdew-Burke-Ernzerhof functionals,” *Phys. Rev. B* (1998).
- ²⁹ H. J. Monkhorst and J. D. Pack, “Special points for Brillouin-zone integrations,” *Physical Review B* **13**, 5188–5192 (1976).
- ³⁰ D. M. Ceperley and B. J. Alder, “Ground state of the electron gas by a stochastic method,” *Physical Review Letters* **45**, 566–569 (1980).
- ³¹ J. P. Perdew *et al.*, “Restoring the density-gradient expansion for exchange in solids and surfaces,” *Phys Rev Lett* **100**, 136406 (2008).
- ³² A. Gulans *et al.*, “Exciting: A full-potential all-electron package implementing density-functional theory and many-body perturbation theory,” *J Phys Condens Matter* **26**, 363202 (2014).
- ³³ M. Gmitra, S. Konschuh, C. Ertler, C. Ambrosch-Draxl, and J. Fabian, “Band-structure topologies of graphene: Spin-orbit coupling effects from first principles,” *Physical Review B* **80** (2009).
- ³⁴ M. Liebmann *et al.*, “Giant Rashba-type spin in ferroelectric GeTe(111),” *Adv Mater* **28**, 560–565 (2016).
- ³⁵ K. S. Novoselov, A. K. Geim, S. V. Morozov, D. Jiang, Y. Zhang, S. V. Dubonos, I. V. Grigorieva, and A. A. Firsov, “Electric field effect in atomically thin carbon films,” (2014).
- ³⁶ B. P. Bahuguna, L. K. Saini, B. Tiwari, and R. O. Sharma, “Electric field induced insulator to metal transition in a buckled GaAs monolayer,” *RSC Adv.* **6**, 52920–52924 (2016).